SI: Atomistic understanding of the $LiNiO_2$-NiO_2 phase diagram from experimentally-guided lattice models

Markus Mock,[a‡] Matteo Bianchini,[a,b‡] Sabrina Sicolo,[*a], François Fauth,[c] Karsten Albe[d]

CONTENTS

[a] BASF SE, Carl-Bosch-Strasse 38, 67056 Ludwigshafen am Rhein, Germany
[b] Battery and Electrochemistry Laboratory, Institute of Nanotechnology, Karlsruhe Institute of Technology (KIT), Hermann-von-Helmholtz-Platz 1, 76344 Eggenstein-Leopoldshafen, Germany
[c] CELLS – ALBA synchrotron, Cerdanyola del Vallés, 08290 Barcelona, Spain
[d] Technische Universitaet Darmstadt, Institut fuer Materialwissenschaft, Fachgebiet Materialmodellierung, Otto-Berndt-Str. 3, 64206 Darmstadt, Germany
‡ These authors contributed equally to this work

S1 BENCHMARK STUDIES

Long et al. [Phys. Rev. Mater. 4, 2020, 045401] found that for the discharged system a Hubbard-U correction with a U value of 2.5 eV is needed to reproduce experimental oxide reaction enthalpies with SCAN. We benchmarked our DFT hull against SCAN-rVV10+U (U = 2.5 eV) and PBE-D3+U (U = 6.0 eV as in [Chem. Mater. 2017, 29, 7840-7851]). The results are presented in Figure S1 (top). We find a very good agreement between SCAN-rVV10 and SCAN-rVV10+U, whereas PBE-D3+U returns a shallower hull while preserving its overall shape.

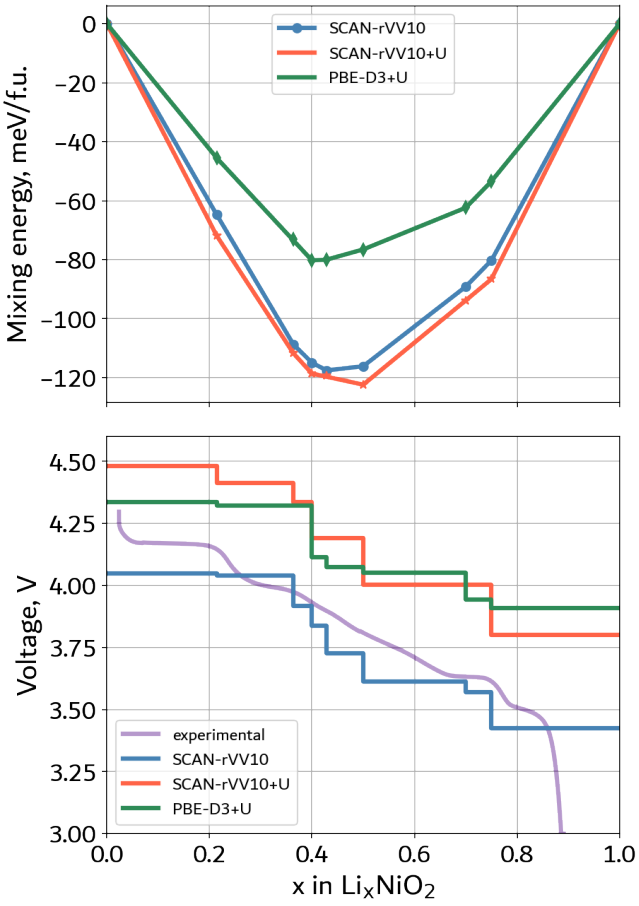

Figure S1

We excluded HSE06 from this benchmark study, as the hybrid functional fails to correctly relax the structure of NiO_2 and leads to its unphysical expansion with a c lattice constant larger than 14.8 Å, which is in clear contradiction with experimental results. The reason for this discrepancy might lie in the need to optimize the mixing parameter α for the given composition, as pointed out in [Phys. Rev. B 92, 115118], but this would prevent the calculation of the hull, which is based on the comparison between consistent energies.

For the same reason, we do not see a justification in utilizing a universal U correction for a set of structures with different compositions where the very atomic species that is affected by the correction experiences changes

in its oxidation state and hence in its electron correlation. Our concern is reinforced if we look at the predicted voltages. To make the comparison between different functionals more straightforward, we computed the 0 K average intercalation voltages for the structures on the hulls:

$$\overline{V}_{x_1,x_2} = -\frac{E(Li_{x_1}NiO_2) - E(Li_{x_2}NiO_2) - (x_1 - x_2)E(Li)}{(x_1 - x_2)F}, x_1 > x_2,$$

which are presented in Figure S1 (bottom).

As already pointed out by Chakraborty et al. [npj Computational Materials 4, 60 (2018)], the U correction introduces a substantial overestimation of the average cell voltage, not only with respect to the SCAN-rVV10 value, but especially to the experimental profile that is shown in light purple.

S2 SIZE EFFECTS AND GEOMETRIC FRUSTRATION

Figure S2 compares isochemical potential lines calculated in $20 \times 20 \times 20$ and $21 \times 21 \times 21$ supercells, and shows that some features depend on the system size. The most notable differences appear at low Li content around $x = 0.25$. Whereas the $20 \times 20 \times 20$ supercell shows one distinct structure at exactly 25 %, the $21 \times 21 \times 21$ supercell shows a solid solution region at 22 % to 27 %. Contrary to conventional size effects, this behavior does not converge with increasing system sizes, but always shows either one of the two outcomes.

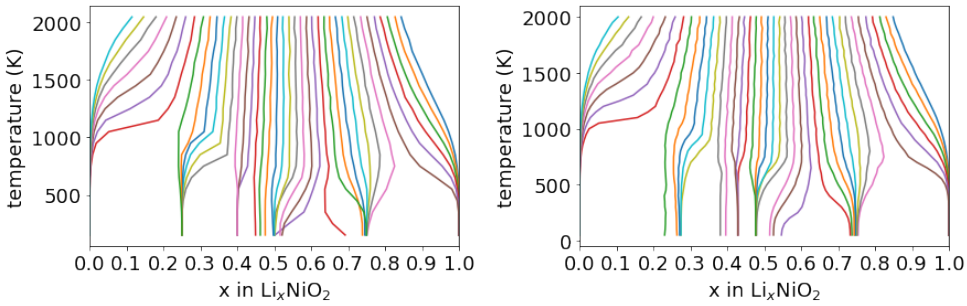

(a) $20 \times 20 \times 20$ supercell **(b)** $21 \times 21 \times 21$ supercell

Figure S2: Isochemical potential lines for stoichiometric Li_xNiO_2. (a) was calculated using a $20 \times 20 \times 20$ supercell, whereas (b) was calculated using a $21 \times 21 \times 21$ supercell. The influence of the cell size on the result does not vanish with increasing cell size and is especially visible at 10 % to 20 %.

It turns out that this behavior is not so much a size effect as a shape effect, and is caused by the geometric frustration of the system. In Figure S3 we present the results of the simulated annealing of $Li_{0.125}NiO_2$ accommodated in supercells with an identical number of atoms but different shapes. Depending on the shape of the supercell, the total energies for the same composition can differ by more than 5 meV/f.u. This artifact is caused by the ability (or inability) of the supercell to accommodate different atomic arrangements. Figure S3b and S3c exemplifies this concept with a two-dimensional model. A certain configuration A fits perfectly in a 6×6 supercell, whereas a different configuration B is forced to form an interface in order to fit in the same supercell. The energetic cost of an interface might artificially penalize configuration B over configuration A, and in the worst case scenario even overturn their relative stabilities. To correctly compare the stability of different atomic arrangements, one should then calculate each configuration in an appropriate supercell.

As a result, the ground state of a system can flip between different structures, depending on which unit cell fits best into the supercell. Increasing the supercell size will in general reduce the influence of the geometric frustration as the ratio between bulk energy difference and interface energy becomes larger. However, in systems where the bulk energy differences are small and/or the interface energies are large, this might require unreasonably large supercells. To circumvent this problem we generated a composite phase diagram, where the extent of every single phase is inferred from a supercell of appropriate size (Figure 5 in the main text).

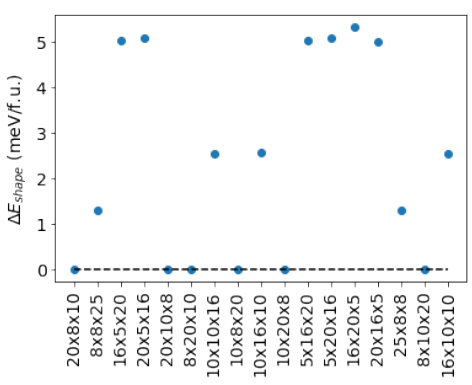

(a) Energy difference between cell shapes

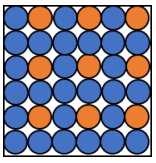

(b) Configuration A

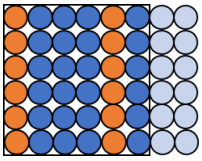

(c) Configuration B

Figure S3: Origin of geometric frustration. (a) Total energies of $Li_{0.125}NiO_2$ in supercells with an identical number of atoms but different shapes; (b) Configuration A fits smoothly inside a 6×6 cell, whereas (c) configuration B is forced to create an interface. This could favour configuration A over configuration B even though the energy of configuration B might be lower in appropriately sized supercells.

S3 OPERANDO XRD AND REFINEMENT

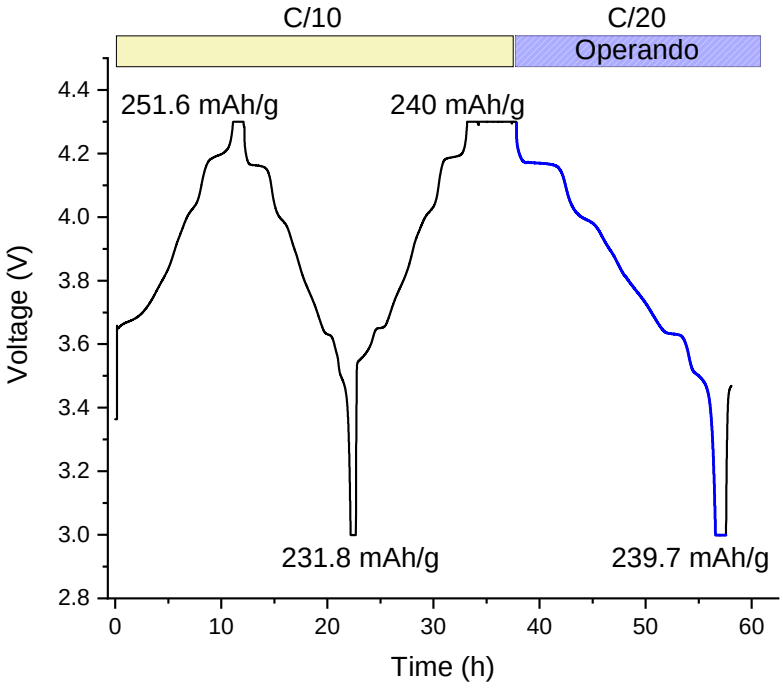

Figure S4: Time-Voltage curve recorded during the operando XRD experiment at the ALBA synchrotron. The first cycle and second charge were measured at C/10 rate prior to the actual operando experiment (C/20 rate).

Table S1: Structural parameters obtained from Rietveld refinement of synchrotron XRD data of $LiNiO_2$.

S.G.: $R\bar{3}m$, Z = 6

$a = 2.87806(3)$ Å
$c = 14.1996(1)$ Å
$V = 101.860(1)$ Å^3

$R_{Bragg} = 1.72\,\%$
$R_{wp} = 9.2\,\%$
$\chi^2 = 11.2$

		Atomic positions				
Atom	Wyckoff position	x/a	b/y	c/z	SOF	B_{iso}
O	6c	0	0	0.2588(2)	1	0.81(5)
Ni	3a	0	0	0	1	0.29(1)
Li	3b	0.5	0.5	0.5	$1-0.024(3)$	0.6(2)
Ni	3b	0.5	0.5	0.5	0.024(3)	0.6(2)

Table S2: Structural parameters obtained from Rietveld refinement of XRD data of $LiNi_{0.95}Al_{0.05}O_2$ (Cu $K_{\alpha 1}$ wavelength).

S.G.: $R\bar{3}m$, Z = 6

$a = 2.8727(1)$ Å
$c = 14.2071(3)$ Å
$V = 101.533(3)$ Å^3

$R_{Bragg} = 3.21\,\%$
$R_{wp} = 13.3\,\%$
$\chi^2 = 2.87$

		Atomic positions				
Atom	Wyckoff position	x/a	b/y	c/z	SOF	B_{iso}
O	6c	0	0	0.2581(3)	1	0.8(1)
Ni	3a	0	0	0	0.95(—)	0.31(6)
Al	3a	0	0	0	0.05(—)	0.31(6)
Li	3b	0.5	0.5	0.5	$1-0.030(3)$	1.4(6)
Ni	3b	0.5	0.5	0.5	0.030(3)	1.4(6)

Table S3: Structural parameters obtained from Rietveld refinement of XRD data of $Li_{0.96}Ni_{1.04}O_2$ (Cu $K_{\alpha 1}$ wavelength).

S.G.: $R\bar{3}m$, Z = 6

$a = 2.8804(1)$ Å
$c = 14.2007(3)$ Å
$V = 102.030(3)$ Å^3

$R_{Bragg} = 2.50\,\%$
$R_{wp} = 10.9\,\%$
$\chi^2 = 3.21$

		Atomic positions				
Atom	Wyckoff position	x/a	b/y	c/z	SOF	B_{iso}
O	6c	0	0	0.2584(2)	1	0.87(7)
Ni	3a	0	0	0	1	0.36(3)
Li	3b	0.5	0.5	0.5	$1-0.048(3)$	0.9(2)
Ni	3b	0.5	0.5	0.5	0.048(3)	0.9(2)

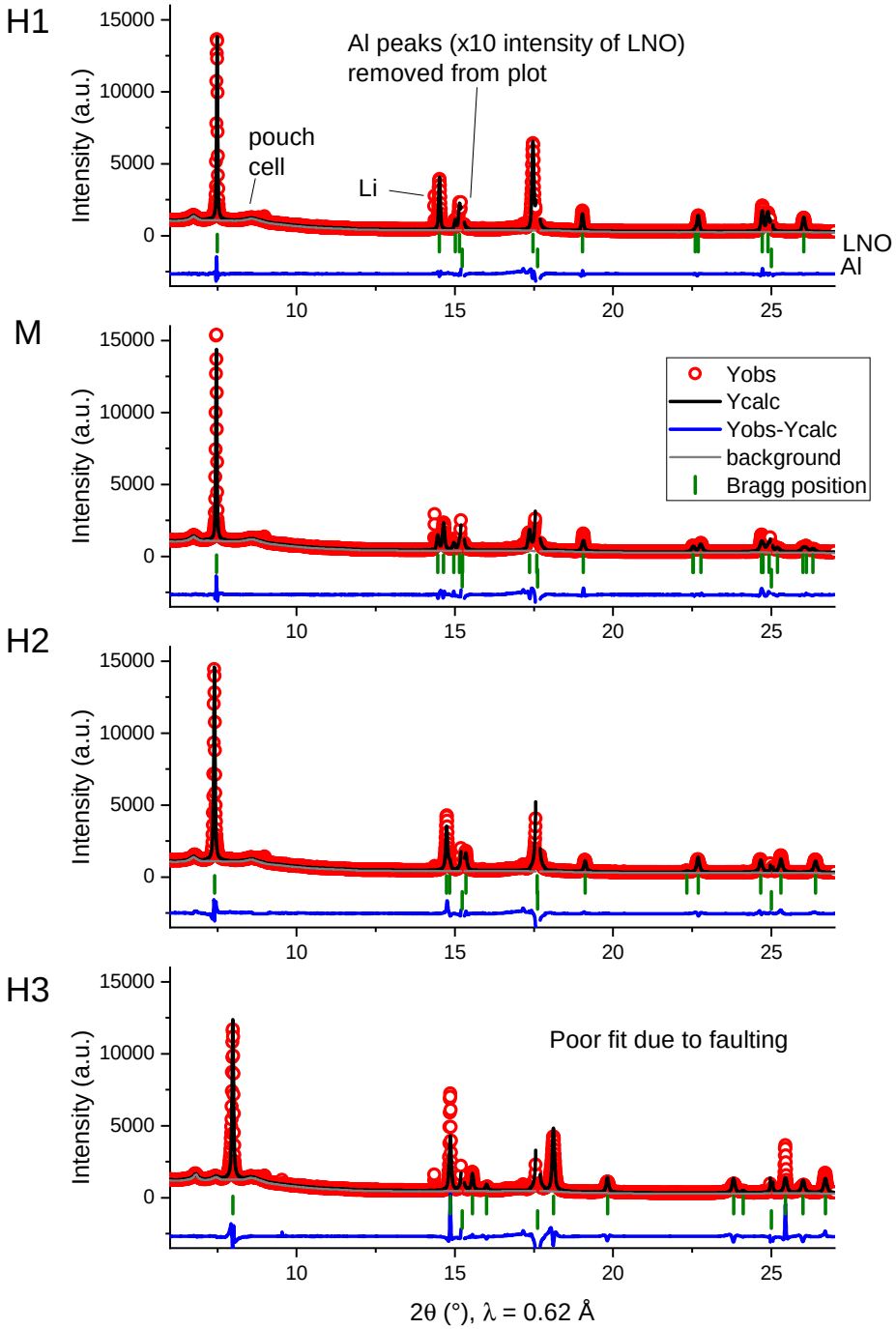

Figure S5: Examples of Rietveld refinement carried out against synchrotron XRD patterns measured operando. The bumps in the background at low angles are due to the amorphous polymeric pouch cell material. Crystalline peaks of Li metal can also be distinguished but were not included in the fit. Aluminum from the pouch cell and current collector was refined with the LeBail method, but omitted from the figure because of its high intensity (about 10 times that of the LNO peaks).

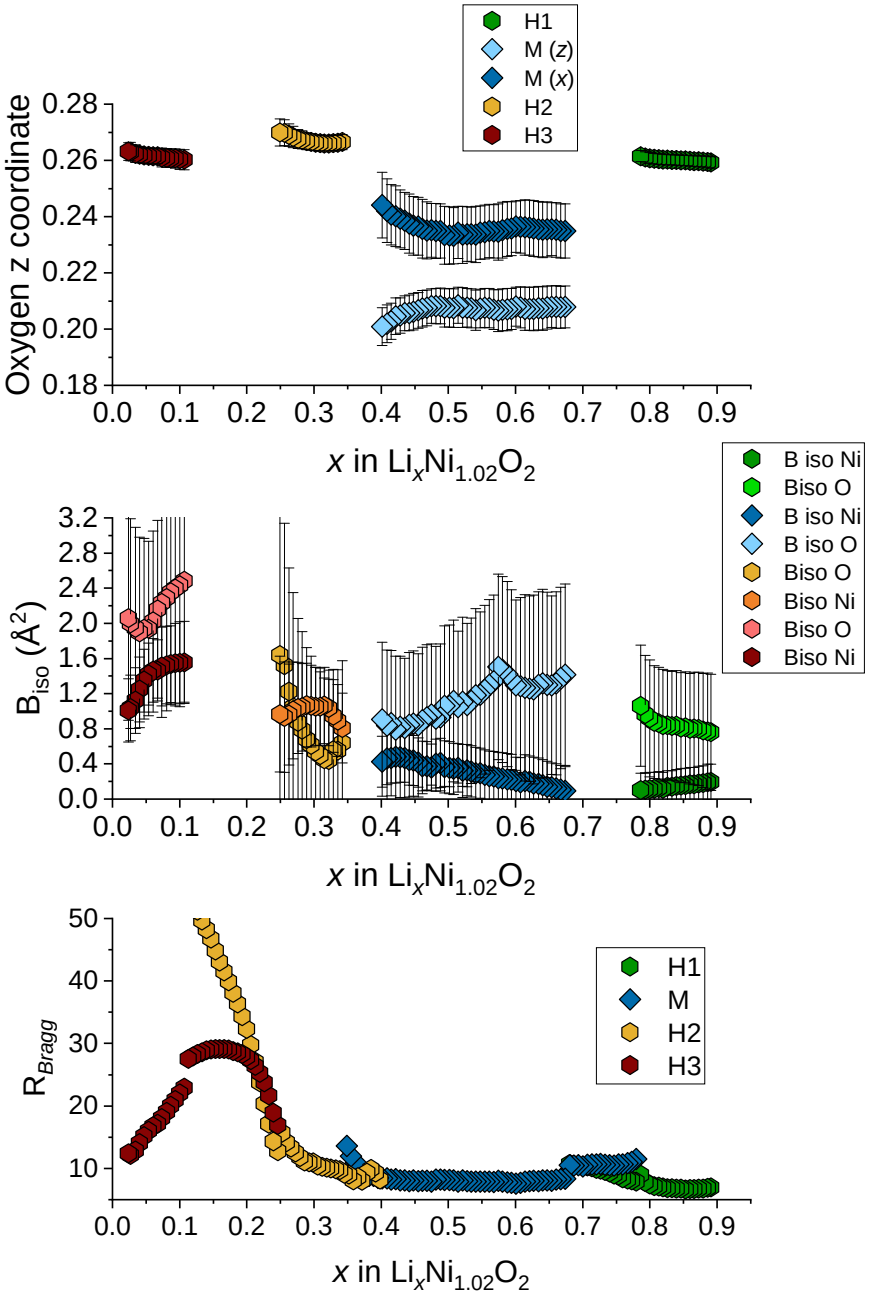

Figure S6: Structural parameters obtained from Rietveld refinement. Parameters were refined in the single-phase domains and fixed in the two-phase ones. Ni site occupancy was fixed in all sites; Li site occupancy was fixed to the average value expected for a given single-phase domain because of the low sensitivity of X-rays to Li. It can be observed that the goodness of fit parameter R_{Bragg} is satisfactory for the H1, M and H2 phases, but it worsens significantly during the H2-H3 and H3 domains due to faulting.

S4 ABSOLUTE LATTICE PARAMETERS

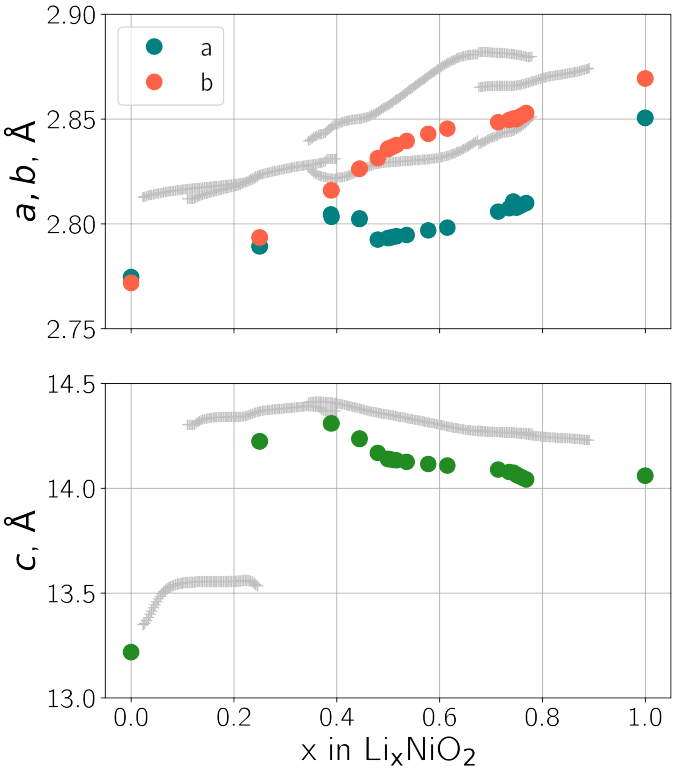

Figure S7: Cluster-expanded lattice constants of Li_xNiO_2 as a function of lithium content at 300 K. Experimental values from Figure 3b are overlayed as light grey crosses. Note that the experimental x values are calculated based on the $Li_{0.98}Ni_{1.02}O_2$ stoichiometry.

S5 LI-VACANCY ORDERINGS

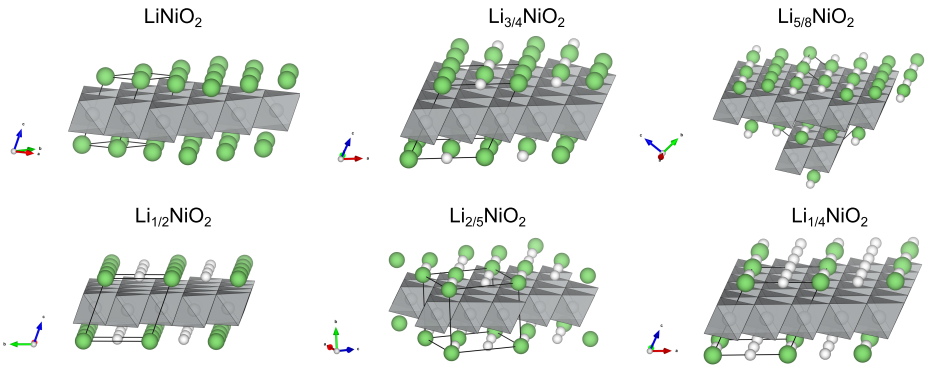

Figure S8: Three-dimensional view of the crystal structures and Li-vacancy orderings reported in Figure 6. Li ions and vacancies are depicted as green and white spheres, respectively, while Ni octahedra are grey. Unit cells have not been standardized.

S5.1 Li-vacancy ordering of $Li_{0.215}Ni_{1.02}O_2$

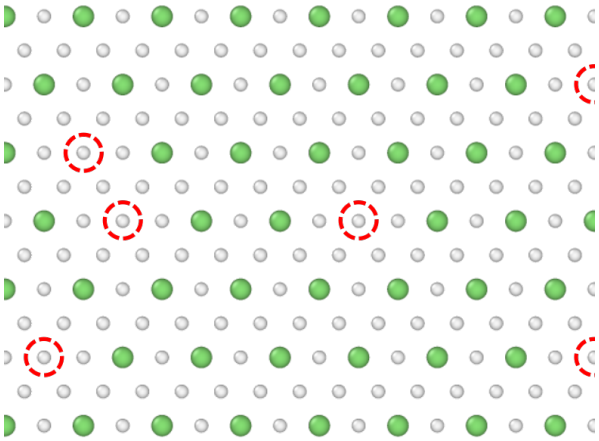

Figure S9: The stable $Li_{0.215}Ni_{1.02}O_2$ phase is a defective version of $Li_{0.25}NiO_2$: the system tries to install the notable Li ordering of alternating empty and half-empty rows despite the presence of pinned vacancies (dashed circles) that are prevented from hosting Li.

S6 KINETIC EFFECTS AT HIGH LI CONTENT

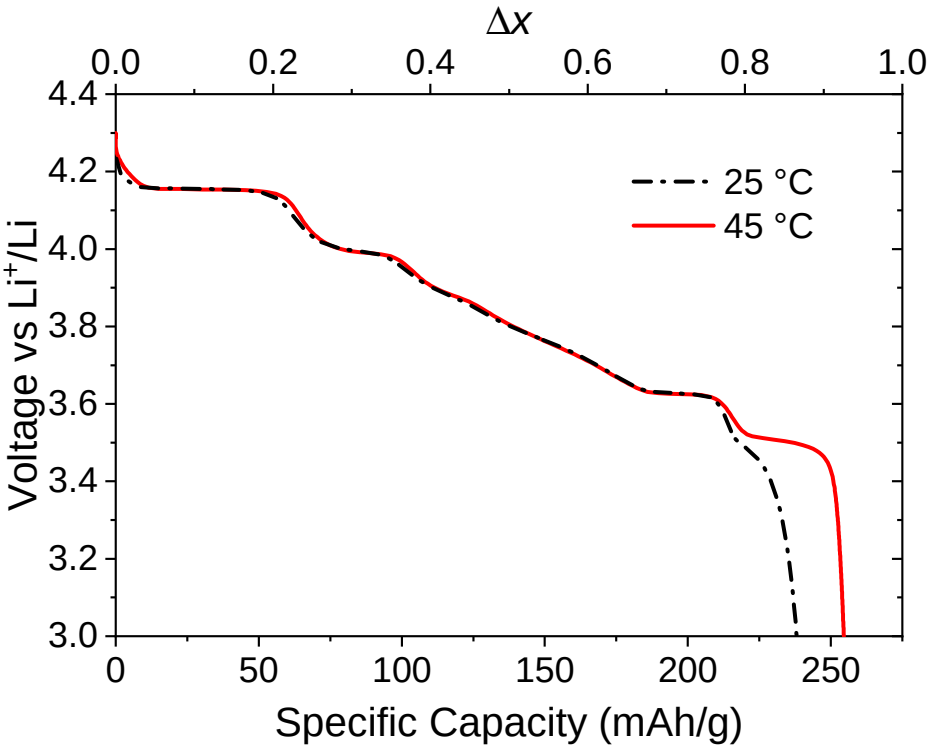

Figure S10: Capacity-Voltage curve of LNO cycled at C/20 rate at 45 °C and 25 °C. The former exhibits additional capacity located in a plateau at 3.5 V, which is kinetically hindered in the latter.